Hot-Electron Energy Deposition in CO_2-Laser-Irradiated Targets Consistent with Magnetic-Field-Induced Surface Transport

J. C. Kieffer, H. Pépin, M. Piché, J. P. Matte, T. W. Johnston, P. Lavigne, and F. Martin
Institut National de la Recherche Scientifique-Energie, Université du Québec, Varennes, Québec J0L 2P0, Canada

and

R. Decoste
Institut de Recherche d'Hydro-Québec, Varennes, Québec J0L 2P0, Canada
(Received 29 October 1982; revised manuscript received 17 January 1983)

Hard-x-ray continuum spectra from high-Z tracers are used to obtain lateral and axial energy-deposition profiles by hot electrons in CO_2-laser-irradiated slab targets. The interpretation of the results emphasizes a local direction of incidence of the hot electrons on the target and an energy-deposition pattern which are consistent with self-generated magnetic fields.

PACS numbers: 52.25.Fi, 52.25.Ps, 52.50.Jm

At sufficiently high intensities the interaction of a long-wavelength laser beam with a target is completely dominated by suprathermal electrons, generated mainly through resonance absorption at the critical density, and predominantly emitted in the corona. The hot electrons which are drawn back into the target by space-charge electric fields transport inward a fraction of the incident laser energy. Thus the hot-electron absorption in a thick shell of low-Z material could in principle be used as a driving mechanism for the shell compression of laser fusion targets. Features of the transport process have been addressed at least qualitatively in several experiments.[1-10] Recently, the trajectories of hot electrons in self-generated magnetic fields have been computed and surface transport has been shown to be dominated by these magnetic fields.[11] In this paper we present a consistent set of quantitative data on electron transport in CO_2-laser-irradiated slab targets which demonstrates the effects of self-generated magnetic fields on the hot-electron trajectories and on the energy-deposition pattern.

Lateral and axial hot-electron energy-deposition profiles are inferred from the local hard-x-ray continuum emitted by hot electrons decelerated in the dense target material. High-Z tracing-material techniques are used to obtain the local emission. Besides, angular distribution of x rays yields direct information on the electron direction of incidence on the target surface. At high irradiances, we find that the electrons deposit most of their energy at oblique angles on the target surface and that the axial energy-deposition profile is in good agreement with a planar semi-isotropic source of incident electrons penetrating the target surface. At low irradiances, the incident electrons appear to be normal to the target surface. A consistent pattern of local energy deposition at high irradiance is obtained from the lateral transport measurements. Near the focal spot, the hot electrons penetrate the target at near-normal incidence, are less energetic, and transport within 1 mm diam only 10% of the total deposited energy. Away from the focal spot, over a very large area (≥ 1 cm^2), the hot electrons are increasingly energetic and incident at oblique angles. All these results are consistent with transport dominated by self-generated magnetic fields.

The study was carried out with a CO_2 laser facility giving a 50-J, 1.2-nsec (full width at half maximum) pulse. The experiments described were made at energy levels up to 15 J with a laser beam incident at 28°, focused onto the target by a $f/1.5$, 15-cm focal length, off-axis parabolic mirror. At best focus, 50% of the energy was contained in a 120-μm-diam spot producing irradiances up to 0.6×10^{14} W cm^{-2}. 30% of the laser energy is absorbed.[3] The time- and space-integrated continuum x-ray emission is recorded with nine K-edge filter detectors[12] covering the 1-70-keV range.

Hot electrons incident on the target surface are characterized by their direction of incidence and by their energy distribution which is assumed to be of the form $f(E_0) = AE_0^{1/2}\exp(-E_0/kT_e)$. The direction of incidence is determined by fitting experimental data with calculated angular distrib-

ution of hard-x-ray emission at various photon energies. The calculation includes a relativistic bremsstrahlung cross section differential in photon direction and energy,[13] involves electrons with arbitrary direction of incidence,[14] and takes into account electron energy and scattering losses. The parameters A and T_e can be inferred from the x-ray spectra. Figure 1 presents, at two irradiances, the angular distribution of hard x rays spatially integrated over the target surface and emitted in a plane normal to a thick CH slab. At low irradiances, the strong anisotropy is best reproduced (hatched region) with electrons at normal incidence. This is consistent with the existence of weak magnetic fields and subsequent near-normal incidence of the returning hot electrons. The slight anisotropy at higher irradiances is best described by a planar semi-isotropic source of hot electrons incident on the target. Indeed, the electrons which are radially convected by the magnetic fields penetrate into the target in a manner which involves a considerable distribution of angles of incidence with respect to the target normal; hence, the incident electron source, spatially integrated over the target surface, is measured to be semi-isotropic. We will see below that the high-irradiance result is consistent with most of the electrons being incident at oblique angles away from the focal spot and a small fraction of the electrons at normal incidence near the focal spot.

Spatially resolved x-ray spectra are inferred from the local hard-x-ray emission detected with high-Z tracing-material techniques. The inward resolution is obtained with increasing thickness of low-Z plastic deposited on a high-Z substrate [inset in Fig. 2(a)]. The lateral resolution across the target surface is obtained with gold disks of various diameters deposited on a lower-Z aluminum substrate [Fig. 2(b)]. In all cases, a 0.1-μm-thick CH overcoat guarantees that the plasma dynamics is always controlled by C and H ions. Figure 2 shows reduced x-ray spectra emitted from the gold material only, for various thicknesses of plastic overcoats or for gold disks of various diameters. The experimentally measured x-ray data, taken at 45° from the target surface, are reduced to the x-ray emission from the gold only by use of the prescription described in Ref. 9. One can directly obtain the local electron energy distribution $g(E)$ below various plastic depths and/or within a given radius around the focal spot by fitting spatially resolved x-ray spectra such as those of Fig. 2 with bremsstrahlung emission calculations involving $g(E)$. The calculations are performed with the bremsstrahlung cross section[13] integrated over all directions, and take into account the electron energy and scattering losses, the effective Z seen by an electron along its path, and photon reabsorption within the high-Z target. When required, a correction must be introduced for the anisotropy of x-ray emission. The hot-electron energy locally deposited is obtained by

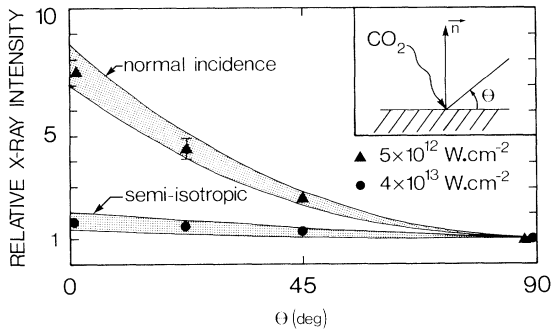

FIG. 1. Experimental and theoretical angular distributions of 30-keV x rays emitted from a thick CH slab. A perpendicular source of incident electrons with T_e = 11 keV gives the best fit to the data at low irradiances. A semi-isotropic source with T_e = 17 keV is required at higher irradiances. In both cases the energy distribution is $f(E_0) = AE^{1/2}\exp(-E_0/kT_e)$. The hatched region for the theoretical predictions reflects the uncertainty due to scattering and energy losses of the electrons in the solid.

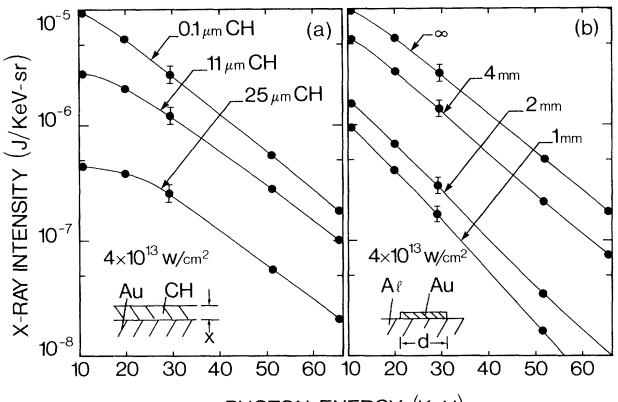

FIG. 2. Local hard-x-ray gold spectra obtained with the high-Z tracing material technique. (a) Various layers of low-Z plastic are deposited on a gold-slab substrate. (b) Gold disks of various diameters are deposited on an aluminum-slab substrate. A 0.1-μm-CH overcoat quarantees that the hot-plasma dynamics is always controlled by C and H ions.

integration of $g(E)E$.

The results obtained with axial resolution enable us to characterize the incident electron source spatially integrated over the target surface. Figure 3 shows the electron energy deposited in a gold substrate below various thicknesses of CH. The solid lines are theoretical predictions of the incident hot-electron energy transmitted below a given depth of plastic, for two types of incidence of the electrons on the target and for the same energy distribution, $f(E_0) = AE_0^{1/2}\exp(-E_0/kT_0)$. The planar semi-isotropic source energy-deposition curve is obtained by use of the electron transport calculation of Spencer.[15,16] For the normal incidence we use a simple analytical model,[14] which gives values of transmitted energy in agreement with those obtained from the Spencer method. At $I \sim 4\times10^{13}$ W cm^{-2}, the experimental values agree very well with the predictions of the semi-isotropic model. The hot electrons trapped in the magnetic field over large distances penetrate the target mostly at oblique incidence and deposit inward approximately 9% of the laser energy or 30% of the absorbed energy; the balance of the absorbed energy appears essentially in fast ions. At $I \sim 5\times10^{12}$ W cm^{-2}, we verify that the normal-incidence model describes the experimental results. The fraction of laser energy carried inward is now ~15%, in agreement with the fact that the electrons return directly back towards the target losing less energy to the ions.[17]

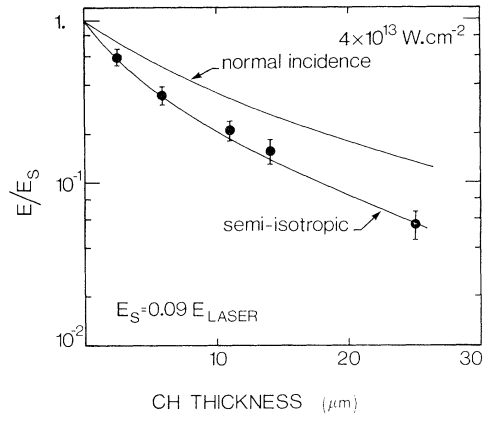

FIG. 3. Fraction of incident hot-electron energy transmitted below various plastic thicknesses. The solid lines are theoretical calculations with two types of sources (perpendicular and semi-isotropic) and the same energy distribution, $f(E_0) = AE^{1/2}\exp(-E_0/kT_e)$. At $I = 4\times10^{13}$ W cm^{-2}, $T_e = 17$ keV and 9% of the incident laser energy is transported inward by hot electrons.

The energy-deposition pattern across the target surface is obtained from measurements involving both axial and lateral resolution. Figure 4(a) shows the hot-electron energy deposited within a given radius either below 11 μm of plastic or on the target surface (0.1 μm CH) at 4×10^{13} W cm^{-2}. In either case the lateral transport extends up to 6 or 7 mm from the local spot. Figure 4(b) gives the radial dependence of hot-electron temperature on the target surface; the incident electrons appear to be colder near the focal spot. The comparison of the two curves in Fig. 4(a) shows that electrons incident at large distances from the focal spot lose more energy in 11 μm of plastic than colder electrons incident at small distances from the focal spot. In other words, the fraction of energy transmitted below 11 μm of plastic is greater near the focal spot than further away. Therefore, referring to Fig. 3, it appears that electrons are incident normal to the target near the focal spot but that they penetrate at an oblique incidence away from the laser axis. This pattern of energy deposition is perfectly consistent with magnetic-field-induced surface transport. Indeed, lower-energy electrons are reflected back to the target near the focal spot without being caught in the magnetic field; they will have a near-normal incidence and the local electron temperature will be reduced. More energetic electrons are convected far away and penetrate the target obliquely. Since at high irradiances most of the incident hot-electron energy is delivered to the target away from the focal spot, the spatially integrated source is

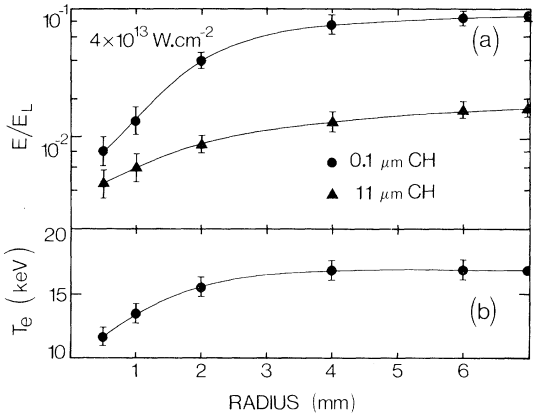

FIG. 4. (a) Radial distribution of electron energy at the target surface (circles) and 11 μm below the surface (triangles) in relative units. E_L is the incident laser energy. (b) Radial dependence of T_e across the target surface.

measured to be semi-isotropic. Self-consistently, at low irradiances, we find that the incident electrons remain close to the focal spot with a near-normal incidence, since the magnetic field should be quite reduced.

In short, the x-ray angular-distribution and axial-transport measurements show the sensitivity of energy deposition to the direction of incidence of the electrons, and hence to the magnetic fields. Results obtained with both axial and lateral resolution give the local energy-deposition pattern which can be consistently interpreted in the light of the self-generated magnetic fields.

The authors want to thank F. Amiranoff and N. Burnett for fruitful discussions and wish to acknowledge the continuing excellent technical support of J. Gauthier, P. P. Mercier, F. Poitras, and J. G. Vallée. This research was supported in part by the Natural Sciences and Engineering Research Council of Canada.

[1]K. B. Mitchel and R. P. Godwin, J. Appl. Phys. 48, 3851 (1977).

[2]J. Hares, J. Kilkenny, M. M. Key, and J. G. Lunmey, Phys. Rev. Lett. 42, 1216 (1979).

[3]J. C. Kieffer *et al.*, Phys. Rev. Lett. 44, 1128 (1980).

[4]R. S. Marjoribanks, M. D. J. Burgess, G. D. Enright, and M. C. Richardson, Phys. Rev. Lett. 45, 1798 (1980).

[5]R. Decoste, J. C. Kieffer, and H. Pépin, Phys. Rev. Lett. 47, 35 (1981).

[6]P. A. Jaanimagi, N. A. Ebrahim, N. H. Burnett, and C. Joshi, Appl. Phys. Lett. 28, 734 (1981).

[7]F. Amiranoff *et al.*, J. Phys. D 15, 2463 (1982).

[8]N. A. Ebrahim, C. Joshi, and H. A. Baldis, Phys. Rev. A 25, 2440 (1982); N. H. Burnett *et al.*, in Proceedings of the Japan–U.S. Seminar on Theory and Application of Multiply Ionized Plasmas Produced by Laser and Particle Beams, Nara, Japan, May 1982 (to be published).

[9]R. Decoste *et al.*, Phys. Fluids 25, 1699 (1982).

[10]M. A. Yates *et al.*, Phys. Rev. Lett. 49, 1702 (1982).

[11]D. W. Forslund and J. V. Brackbill, Phys. Rev. Lett. 48, 1614 (1982); R. Fabbro and P. Mora, Phys. Lett. 90A, 48 (1982).

[12]H. Pépin *et al.*, J. Appl. Phys. 50, 6784 (1979).

[13]H. Kuhlenkampff, M. Scheer, and E. Zietler, Z. Phys. 157, 275 (1959).

[14]J. C. Kieffer, Ph.D. thesis, Université du Québec, Institut National de la Recherche Scientifique–Energie, 1982 (unpublished).

[15]L. V. Spencer, Phys. Rev. 98, 1597 (1955); R. J. Harrach and R. E. Kidder, Phys. Rev. A 23, 887 (1981).

[16]The Bethe-Bloch electron range that we use applies to the penetration of cold matter, but does not differ significantly from the range of energetic electrons (10–200 keV) in a relatively cold (10–100-eV) plasma approaching solid density. A discussion pertinent to this point appears in Rutherford Laboratory Laser Division Annual Report No. RL-79-036, 1979 (unpublished), p. 4.27.

[17]P. Church, F. Martin, H. Pépin, and R. Decoste, J. Appl. Phys. 53, 874 (1982).